18

Spin Photodetector: Conversion of Light Polarization Information into Electric Voltage Using Inverse Spin Hall Effect

Kazuya Ando and Eiji Saitoh
Institute for Materials Research, Tohoku University
Japan

1. Introduction

Recent developments in optical and material science have led to remarkable industrial applications, such as optical data recording and optical communication. The scope of the conventional optical technology can be extended by exploring simple and effective methods for detecting light circular polarization; light circular polarization carries single-photon information, making it essential in future optical technology, including quantum cryptography and quantum communication.

Light circular polarization is coupled with electron spins in semiconductors (Meier, 1984). When circularly polarized light is absorbed in a semiconductor crystal, the angular momentum of the light is transferred to the semiconductor, inducing spin-polarized carriers though the optical selection rules for interband transitions [see Fig. 1(a)]. This process allows conversion of light circular polarization into electron-spin polarization, enabling the integration of light-polarization information into spintronic technologies.

If one can convert electron spin information into an electric signal, light circular polarization information can be measured through the above process. Recently, in the field of spintronics, a powerful technique for detecting electron spin information has been established, which utilizes the inverse spin Hall effect (ISHE) (Saitoh, 2006; Valenzuela, 2006; Kimura, 2007). The ISHE converts a spin current, a flow of electron spins in a solid, into an electric field through the spin-orbit interaction, enabling the transcription of electron-spin information into an electric voltage. This suggests that light-polarization information can be converted into an electric signal by combining the optical selection rules and the ISHE.

This chapter describes the conversion of light circular polarization information into an electric voltage in a Pt/GaAs structure though the optical generation of spin-polarized carriers and the ISHE: the photoinduced ISHE (Ando, 2010).

2. Optical excitation of spin-polarized carriers in semiconductors

When circularly polarized light is absorbed in a semiconductor, the angular momentum of the light is transferred to the material, which polarizes carrier spins in the semiconductor

through the spin-orbit interaction (Meier, 1984). This optical generation of spin-polarized carriers has been a powerful technique for exploring spin physics in direct band gap semiconductors, such as GaAs. In GaAs, the valence band maximum and the conduction band minimum are at Γ with an energy gap E_g = 1.43 eV at room temperature. The valence band (*p* symmetry) splits into fourfold degenerate $P_{3/2}$ and twofold degenerate $P_{1/2}$ states, which lie Δ = 0.34 eV below $P_{3/2}$ at Γ, whereas the conduction band (*s* symmetry) is twofold degenerate $S_{1/2}$ as schematically shown in Fig. 1(a). In the fourfold degenerate $P_{3/2}$ state, holes can occupy states with values of angular momentum m_j = ±1/2, ±3/2, corresponding to light hole (LH) and heavy hole (HH) sates, respectively (see Fig. 1(a)). Let $|J, m_j\rangle$ be the Bloch states according to the total angular momentum *J* and its projection onto the positive *z* axis m_j. The band wave functions can be expressed as listed in Table 1, where $|S\rangle$, $|X\rangle$, $|Y\rangle$, and $|Z\rangle$ are the wave functions with the symmetry of *s*, p_x, p_y, and p_x orbitals. The interband transitions satisfy the selection rule $\Delta m_j = \pm 1$, reflecting absorption of the photon's original angular momentum. The probability of a transition involving a LH or HH state is weighted by the square of the corresponding matrix element connecting it to the appropriate electron state, so that the relative intensity of the optical transition between the heavy and the light hole subbands and the conduction band induced by circularly polarized light illumination is 3. Thus absorption of photons with angular momentum +1 produces three spin-down (m_j = –1/2) electrons for every one spin-up (m_j = +1/2) electron, resulting in an electron population with a spin polarization of 50% in a bulk material, where the HH and LH states are degenerate. The relative transition rates are summarized in Fig. 1(b). Therefore, because of the difference in the relative intensity, a spin-polarized carriers can be generated by the illumination of circularly polarized light. Note that the resulting electron spin is oriented parallel or anti-parallel to the propagation direction of the incident photon.

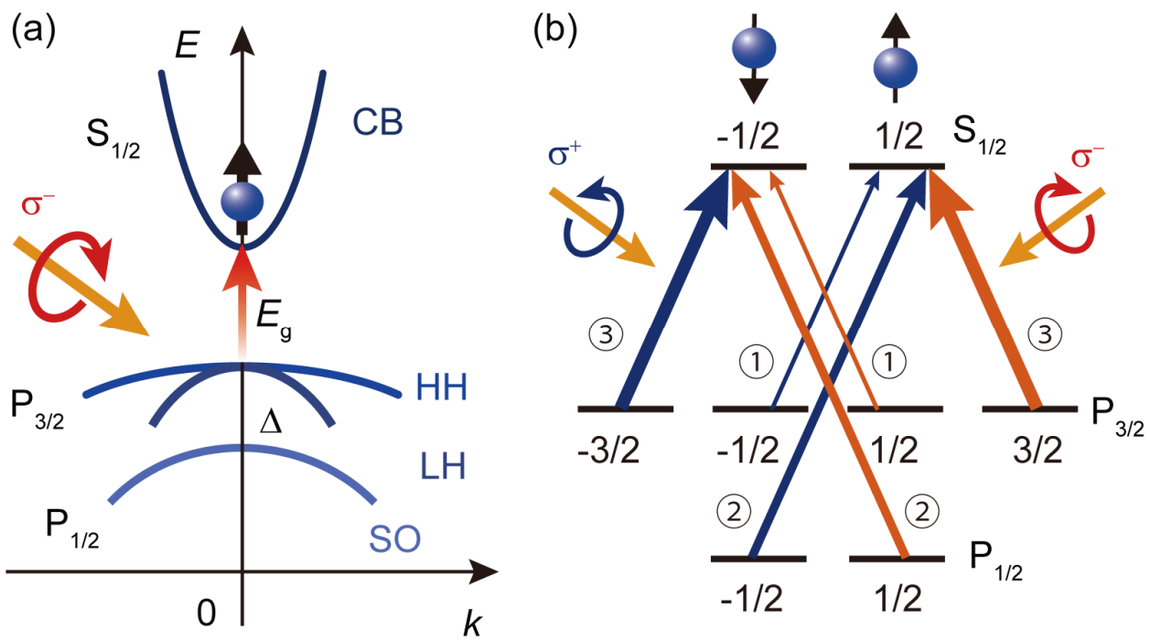

Fig. 1. (a) Optical generation of spin-polarized carriers in semiconductors. (b) Interband transitions for right and left circularly polarized light illumination.

	$\|J, m_j\rangle$	wave function
CB	$\|1/2, 1/2\rangle$	$\|S\uparrow\rangle$
	$\|1/2, -1/2\rangle$	$\|S\downarrow\rangle$
HH	$\|3/2, 3/2\rangle$	$\|(1/2)^{(1/2)}(X+iY)\uparrow\rangle$
	$\|3/2, -3/2\rangle$	$\|(1/2)^{(1/2)}(X-iY)\downarrow\rangle$
LH	$\|3/2, 1/2\rangle$	$\|(1/6)^{(1/2)}[(X+iY)\downarrow+2Z\uparrow]\rangle$
	$\|3/2, -1/2\rangle$	$\|-(1/6)^{(1/2)}[(X-iY)\uparrow-2Z\downarrow]\rangle$
SO	$\|1/2, 1/2\rangle$	$\|-(1/3)^{(1/2)}[(X+iY)\downarrow-Z\uparrow]\rangle$
	$\|1/2, -1/2\rangle$	$\|(1/3)^{(1/2)}[(X-iY)\uparrow+Z\downarrow]\rangle$

Table 1. Wave functions for the conduction band (CB), heavy hole (HH), light hole (LH), and spin-orbit split-off band (SO).

3. Spin current and inverse spin Hall effect

A spin current is a flow of electron spins in a solid. One of the driving forces for a spin current is a gradient of the difference in the spin-dependent electrochemical potential $\nabla\mu_\sigma$ for spin up ($\sigma = \uparrow$) and spin down ($\sigma = \downarrow$). Here, $\mu_\sigma = \mu_\sigma^c - e\phi$, where μ_σ^c is the chemical potential. A current density for spin channel σ is expressed as

$$\mathbf{j}_\sigma = \frac{\sigma_\sigma}{e}\nabla\mu_\sigma, \tag{1}$$

where σ_σ is the electrical conductivity for spin up ($\sigma = \uparrow$) and spin down ($\sigma = \downarrow$) channel. Here, a charge current, a flow of electron charge, is the sum of the current for $\sigma = \uparrow$ and $\downarrow$ as $\mathbf{j}_c = \mathbf{j}_\uparrow + \mathbf{j}_\downarrow$:

$$\mathbf{j}_c = \frac{1}{e}\nabla\left(\sigma_\uparrow\mu_\uparrow + \sigma_\downarrow\mu_\downarrow\right). \tag{2}$$

This flow is schematically illustrated in Fig. 2(a). This flow carries electron charge while the flow of spins is cancelled. In contrast, the opposite flow of $\mathbf{j}_\uparrow$ and $\mathbf{j}_\downarrow$, $\mathbf{j}_s = \mathbf{j}_\uparrow - \mathbf{j}_\downarrow$, or

$$\mathbf{j}_s = \frac{1}{e}\nabla\left(\sigma_\uparrow\mu_\uparrow - \sigma_\downarrow\mu_\downarrow\right), \tag{3}$$

carries electron spins without a charge current. This is a spin current. In nonmagnetic materials, a spin current is expressed as $\mathbf{j}_s = (\sigma_N/2e)\nabla(\mu_\uparrow - \mu_\downarrow)$, since the electrical conductivity is spin-independent: $\sigma_\uparrow = \sigma_\downarrow = \sigma_N/2$.

Since charge ρ is a conserved quantity, the continuity equation of charge is described as

$$\frac{d}{dt}\rho = -\nabla\cdot\mathbf{j}_c. \tag{4}$$

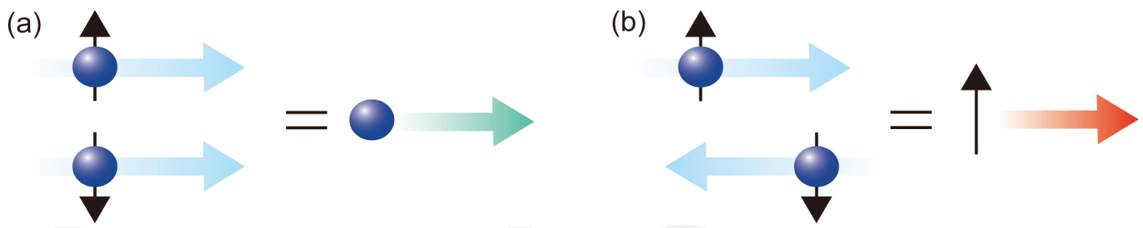

Fig. 2. (a) A schematic illustration of a charge current. (b) A schematic illustration of a spin current.

In contrast, spins are not conserved; a spin current decays typically in a length scale of nm to μm. Therefore, the continuity equation of spins are written as

$$\frac{d}{dt}M_z = -\nabla\cdot\mathbf{j}_s + \mathcal{T}_z, \tag{5}$$

where M_z is the z component of magnetization. z is defined as the quantization axis. Here, $\mathcal{T}_z = e(n_\uparrow - \overline{n}_\uparrow)/\tau_{\uparrow\downarrow} - e(n_\downarrow - \overline{n}_\downarrow)/\tau_{\downarrow\uparrow}$ represents spin relaxation. $\overline{n}_\sigma$ is the equilibrium carrier density with spin σ and $\tau_{\sigma\sigma'}$ is the scattering time of an electron from spin state from σ to σ'. Note that the detailed balance principle imposes that $N_\uparrow/\tau_{\uparrow\downarrow} = N_\downarrow/\tau_{\downarrow\uparrow}$, so that in equilibrium no net spin scattering takes place, where N_σ denotes the spin dependent density of states at the Fermi energy. This indicates that, in general, in a ferromagnet, $\tau_{\uparrow\downarrow}$ and $\tau_{\downarrow\uparrow}$ are not the same. In the equilibrium condition, $d\rho/dt = dM_z/dt = 0$, using the continuity equations, one finds the spin-diffusion equations:

$$\nabla^2(\sigma_\uparrow\mu_\uparrow + \sigma_\downarrow\mu_\downarrow) = 0, \tag{6}$$

$$\nabla^2(\mu_\uparrow - \mu_\downarrow) = \frac{1}{\lambda^2}(\mu_\uparrow - \mu_\downarrow), \tag{7}$$

where $\lambda = \sqrt{D\tau_{sf}}$ is the spin diffusion length. $D = D_\uparrow D_\downarrow(N_\uparrow + N_\downarrow)/(N_\uparrow D_\uparrow + N_\downarrow D_\downarrow)$ is the diffusion constant. The spin relaxation time τ_{sf} is given by $1/\tau_{sf} = 1/\tau_{\uparrow\downarrow} + 1/\tau_{\downarrow\uparrow}$. By solving the diffusion equations, one can obtain the spatial variation of spin currents generated by $\mu_\uparrow - \mu_\downarrow$. A spin current generated by $\mu_\uparrow - \mu_\downarrow$ decays as $e^{-\lambda/x}$. Thus a spin current play a key role only in a system with the scale of λ.

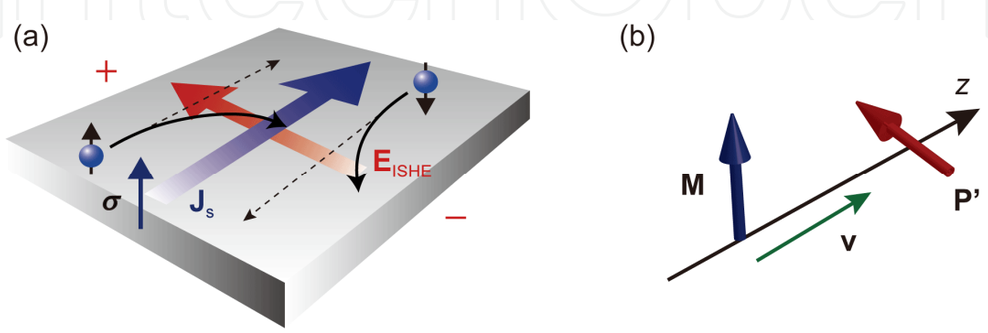

Fig. 3. (a) A schematic illustration of the inverse spin Hall effect. (b) Conversion of magnetic moment **M** into electric polarization **P**'.

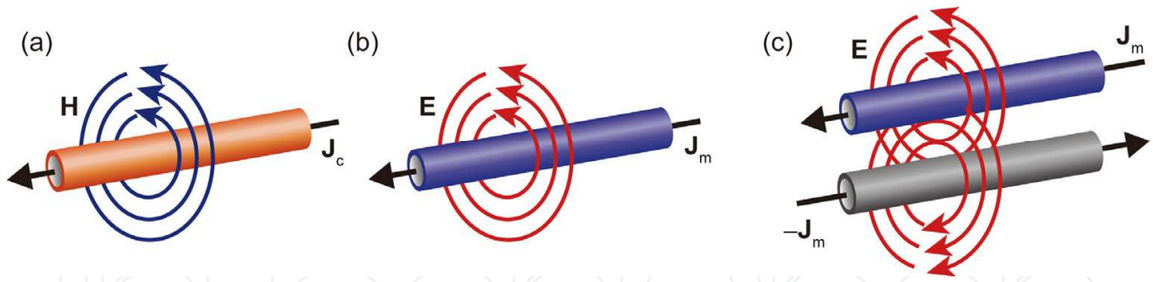

Fig. 4. (a) A schematic illustration of the magnetic-field **H** generation from a charge current $\mathbf{j}_c$ according to Ampere's law. (b) A schematic illustration of the electric-field **E** generation from a hypothetical magnetic-monopole current $\mathbf{j}_m$ according to the electromagnetic duality and Ampere's law. (c) A schematic illustration of the electric-field **E** generation from a pair of hypothetical magnetic-monopole currents, $\mathbf{j}_m$ and $-\mathbf{j}_m$, or a spin current.

A spin current can be detected electrically using the inverse spin Hall effect (ISHE), conversion of a spin current into an electric field [see Fig. 3(a)]. The ISHE has the same symmetry as that of the relativistic transformation of magnetic moment into electric polarization, which is derived from the Lorentz transformation, as follows. Consider a magnet with the magnetic moment **M** moving at a constant velocity **v** along the *z* axis with respect to an observer [see Fig. 3(b)]. This motion of the magnet is a flow of angular momentum, meaning an existence of a "spin current". In the observer's coordinate system, the Lorentz transformation converts a part of this magnetic moment **M** into an electric dipole moment **P**' as

$$\mathbf{P}' = -\frac{1}{\sqrt{1-(v/c)^2}}(\epsilon_0 \mathbf{v} \times \mathbf{M}), \tag{8}$$

where c and ε_0 are the light velocity and the electric constant, respectively. This indicates that electric polarization perpendicular to the direction of the magnetic-moment velocity is induced.

This electric-polarization generation can also be regarded as the spin-current version of Ampere's law as follows. As shown in Fig. 4(a), when a charge current $\mathbf{j}_c$ flows, a circular magnetic field **H** is induced around the charge current, according to Ampere's law: rot**H** = $\mathbf{j}_c$. If a hypothetical magnetic monopole flows, a circular electric field **E** is expected to be induced around the monopole current $\mathbf{j}_m$ according to rot**E** = $\mathbf{j}_m$ [see Fig. 4(b)], from the electromagnetic duality. Although this monopole has never been observed in reality, a spin current can be regarded as a pair of the hypothetical monopole currents flowing in the opposite directions along the spin current spatial direction. Therefore, a spin current may generate an electric field and this field is the superposition of the two electric fields induced by this pair of the monopole current, as shown in Fig. 4(c). This spin-current-induced electric field is identical to the field induced by the dipole moment described by Eq. (8).

In this way, electromagnetism and relativity predict that a spin current generates an electric field. According to Eq. (8), however, this electric field is too weak in a vacuum to be detected

in reality. In a solid with strong spin-orbit interaction, in contrast, a similar but strong conversion between spin currents and electric fields appears, which is the ISHE.

In a solid, existence of a spin current can be modelled as that two electrons with opposite spins travel in opposite directions along the spin-current spatial direction $\mathbf{j}_s$, as shown in Fig. 3(a). Here, σ denotes the spin polarization vector of the spin current. The spin-orbit interaction bends these two electrons in the same direction and induces an electromotive force $\mathbf{E}_{ISHE}$ transverse to $\mathbf{j}_s$ and σ, which is the ISHE. The relation among $\mathbf{j}_s$, $\mathbf{E}_{ISHE}$, and σ is therefore given by (Saitoh, 2006)

$$\mathbf{E}_{ISHE} = D_{ISHE}\mathbf{J}_s \times \sigma, \tag{9}$$

where D_{ISHE} is the ISHE efficiency. This equation is similar to Eq. (8) but this effect may be enhanced by the strong spin-orbit interaction in solids.

The ISHE was recently observed using a spin-pumping method operated by ferromagnetic resonance (FMR) and by a non-local method in metallic nanostructures (Saitoh, 2006; Valenzuela, 2006; Kimura, 2007). Since the ISHE enables the electric detection of a spin current, it will be useful for exploring spin currents in condensed matter.

4. Photoinduced inverse spin Hall effect: Experiment

The combination of the optical generation of spin-polarized carriers and the ISHE enables direct conversion of light-polarization information into electric voltage in a Pt/GaAs interface (Ando, 2010). Figure 5(a) shows a schematic illustration of the Pt/GaAs sample. Here, the thickness of the Pt layer is 5 nm. The Pt layer was sputtered on a Si-doped GaAs substrate with a doping concentration of $N_D = 4.7 \times 10^{18}$ cm^{-3}. The surface of the GaAs layer was cleaned by chemical etching immediately before the sputtering. Two electrodes are attached to the ends of the Pt layer as shown in Fig. 5(a). During the measurement, circularly polarized light with a wavelength of $\lambda = 670$ nm and a power of $I_i = 10$ mW was illuminated to the Pt/GaAs sample as shown in Fig. 5(a). In the GaAs layer, electrons with a spin polarization σ along the light propagation direction are excited to the conduction band by the circularly polarized light due to the optical selection rule. Here, note that hole spin polarization plays a minor role in this setup, since it relaxes in ~ 100 fs, which is much faster than the relaxation time of ~ 35 ps for electron spin polarization (Hilton, 2002; Kimel, 2001). This spin polarization of electrons then travels into the Pt layer across the interface as a pure spin current. The injected spin current is converted into an electric voltage by the ISHE in the Pt layer due to the strong spin-orbit interaction in Pt (Ando, 2008). Here, note that the angle of the light illumination to the normal axis of the film plane is set at $\theta_0 = 65°$ to obtain the photoinduced ISHE signal, since the electric voltage due to the photoinduced ISHE is proportional to $j_s \sin\theta_0$ because of the relation $\mathbf{E}_{ISHE} \propto \mathbf{j}_s \times \sigma$, where the spin polarization σ is directed along the light propagation direction. The difference in the generated voltage between illumination with right circularly polarized (RCP) and left circularly polarized (LCP) light, $V^R - V^L$, was measured by a polarization-lock-in technique using a photoelastic modulator operated at 50 kHz. The difference in the intensities between RCP and LCP light incident on the sample was confirmed to be vanishingly small. All the measurements were performed at room temperature at zero applied bias across the junction.

In-plane light illumination angle θ dependence of $V^{\mathrm{R}} - V^{\mathrm{L}}$ for the Pt/GaAs sample is shown in Fig. 5(b), where the in-plane angle θ is defined in Fig. 5(a). Figure 5(b) shows that $V^{\mathrm{R}} - V^{\mathrm{L}}$ varies systematically by changing the illumination angle θ. Notable is that this variation is well reproduced using a function proportional to $\cos\theta$, as expected for the photoinduced ISHE. The relation of the ISHE, $\mathbf{E}_{\mathrm{ISHE}} \propto \mathbf{j}_{\mathrm{s}} \times \sigma$, indicates that the electric voltage due to the photoinduced ISHE is proportional to $|\mathbf{j}_{\mathrm{s}} \times \sigma|_x \propto \cos\theta$, since σ and $\mathbf{j}_{\mathrm{s}}$ are directed along the light propagation direction and the z axis, respectively. Here, $|\mathbf{j}_{\mathrm{s}} \times \sigma|_x$ denotes the x component of $\mathbf{j}_{\mathrm{s}} \times \sigma$ [see Fig. 5(a)]. This electromotive force was found to be disappeared in a Cu/GaAs system, where the Pt layer is replaced by Cu with very weak ISHE, supporting that ISHE is responsible for the observed electric voltage.

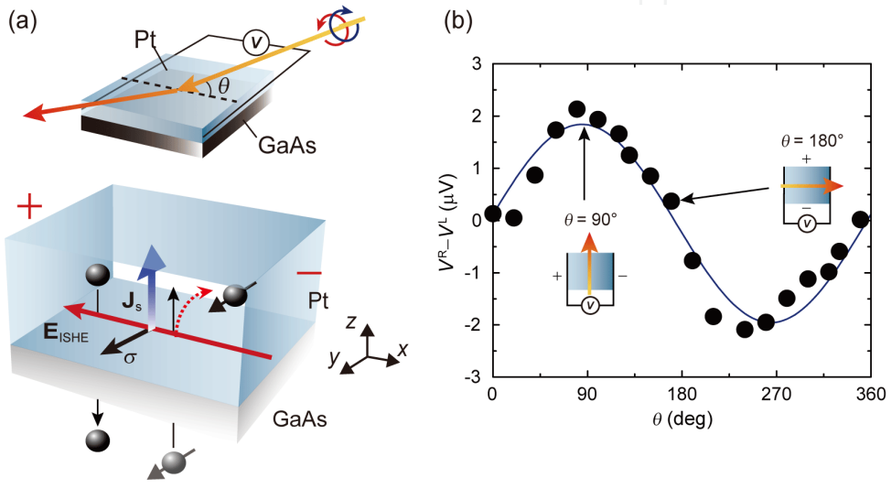

Fig. 5. (a) A schematic illustration of the Pt/GaAs hybrid structure and the photoinduced ISHE in the Pt/GaAs system. (b) In-plane illumination angle θ dependence of $V_{\mathrm{R}}-V_{\mathrm{L}}$ measured for the Pt/GaAs hybrid structure.

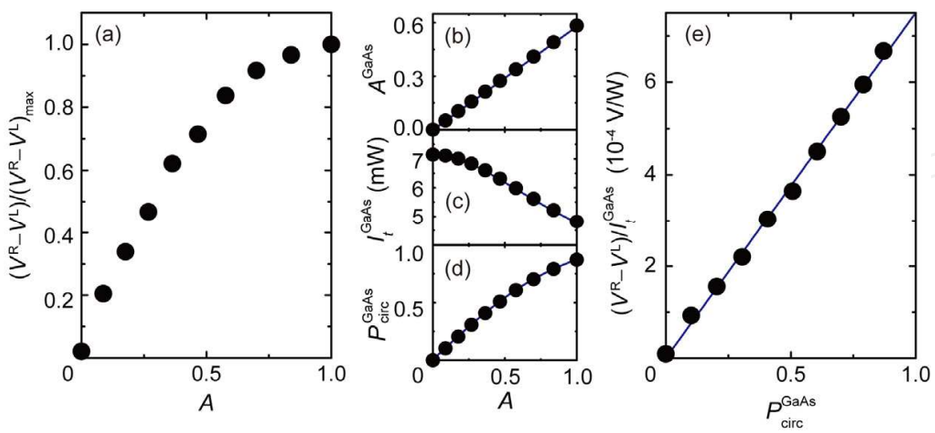

Fig. 6. (a) Ellipticity A of the illuminated light dependence of $V_{\mathrm{R}} - V_{\mathrm{L}}$. (b) A dependence of the ellipticity A^{GaAs} of the light injected into the GaAs layer. (c) A dependence of the intensity I_t^{GaAs} of the light injected into the GaAs layer. (d) A dependence of the degree of circular polarization $P_{\mathrm{circ}}^{\mathrm{GaAs}}$ of the light injected into the GaAs layer. (e) $P_{\mathrm{circ}}^{\mathrm{GaAs}}$ dependence of $(V^{\mathrm{R}} - V^{\mathrm{L}}) / I_{\mathrm{t}}^{\mathrm{GaAs}}$.

The observed electric voltage signal depends strongly on the ellipticity of the illuminated light polarization. Here, the ellipticity A is defined as the ratio of the minor to major radiuses of the elliptically polarized light. Figure 6(a) shows the illuminated-light ellipticity A dependence of $V^{\mathrm{R}} - V^{\mathrm{L}}$. As shown in Fig. 6(a), the $V^{\mathrm{R}} - V^{\mathrm{L}}$ signal increases with the ellipticity A of the illuminated light. This supports that this signal is induced by the photoinduced ISHE, since the angular momentum component of a photon along the light propagation direction is zero (maximized) when $A = 0$ (1).

5. Photoinduced inverse spin Hall effect: Theory

The A dependence of $V^{\mathrm{R}} - V^{\mathrm{L}}$ shown in Fig. 6(a) demonstrates that the electric voltage observed in the Pt/GaAs junction is induced by the circularly polarized light illumination. However, the variation of the electric voltage with respect to A is not straightforward to understand; the $V^{\mathrm{R}} - V^{\mathrm{L}}$ signal is not linear to A. In the following, we discuss in detail on the experimental result by calculating the polarization of the light injected into the GaAs layer.

The propagation of light in a multilayer film is characterized by the optical admittance $Y^{\mathrm{s(p)}} = C^{\mathrm{s(p)}}/B^{\mathrm{s(p)}}$, where s(p) denotes s(p) polarized light. $B^{\mathrm{s(p)}}$ and $C^{\mathrm{s(p)}}$ are expressed as

$$\begin{pmatrix} B^{\mathrm{s(p)}} \\ C^{\mathrm{s(p)}} \end{pmatrix} = \begin{pmatrix} \cos\delta & (i\sin\delta)/\eta_1^{\mathrm{s(p)}} \\ i\eta_1^{\mathrm{s(p)}}\sin\delta & \cos\delta \end{pmatrix} \begin{pmatrix} 1 \\ \eta_2^{\mathrm{s(p)}} \end{pmatrix}, \tag{10}$$

where $\delta = 2\pi n_1 d_1 \cos\theta_1 / \lambda$, $\eta_r^{\mathrm{p}} = n_r(\varepsilon_0/\mu_0)^{1/2}/\cos\theta_r$, and $\eta_r^{\mathrm{s}} = n_r(\varepsilon_0/\mu_0)^{1/2}\cos\theta_r$ (r = 0, 1, 2). Here, n_0, n_1, and n_2 are the complex refractive indices for air, Pt, and GaAs, respectively. d_1 is the thickness of the Pt layer and θ_r is the incident angle of the light defined as shown in Fig. 7. Using $B^{\mathrm{s(p)}}$ and $C^{\mathrm{s(p)}}$, the transmittance $T^{\mathrm{s(p)}} \equiv I_{\mathrm{t}}^{\mathrm{s(p)}} / I_{\mathrm{i}}^{\mathrm{s(p)}}$ and the transmission coefficient $\tau^{\mathrm{s(p)}} \equiv E_{\mathrm{t}}^{\mathrm{s(p)}} / E_{\mathrm{i}}^{\mathrm{s(p)}}$ are obtained as

$$T^{\mathrm{s(p)}} = \frac{4\eta_0^{\mathrm{s(p)}}\Re[\eta_2^{\mathrm{s(p)}}]}{(\eta_0^{\mathrm{s(p)}}B^{\mathrm{s(p)}} + C^{\mathrm{s(p)}})(\eta_0^{\mathrm{s(p)}}B^{\mathrm{s(p)}} + C^{\mathrm{s(p)}})^*}, \tag{11}$$

$$\tau^{\mathrm{s}} = \frac{2\eta_0^{\mathrm{s}}}{\eta_0^{\mathrm{s}}B^{\mathrm{s}} + C^{\mathrm{s}}}, \quad \tau^{\mathrm{p}} = \frac{2\eta_0^{\mathrm{p}}}{\eta_0^{\mathrm{p}}B^{\mathrm{p}} + C^{\mathrm{p}}}\frac{\cos\theta_0}{\cos\theta_2}, \tag{12}$$

where $I_{\mathrm{i(t)}}^{\mathrm{s(p)}}$ and $E_{\mathrm{i(t)}}^{\mathrm{s(p)}}$ are the illuminated (transmitted) light intensity and the amplitude of the electric field of s(p) polarized light [see Fig. 7], respectively. Here, $\Re[\eta_2^{\mathrm{s(p)}}]$ is the real part of $\eta_2^{\mathrm{s(p)}}$. Using Eqs. (11) and (12) with the parameters shown in Table 2, the transmittance $T^{\mathrm{s(p)}}$ and the transmission coefficient $\tau^{\mathrm{s(p)}}$ for the Pt/GaAs system are obtained as shown in Table 3. The calculated transmission coefficients $\tau^{\mathrm{s(p)}}$ show that the transmission of the s and p polarized light is different. This indicates that the ellipticity of the illuminated to the sample is changed during the propagation of the film. The relation between the ellipticity A^{GaAs} of the light injected into the GaAs layer and the ellipticity A of the illuminated light is shown in Fig. 6(b). Here, A^{GaAs} is obtained using

$A^{\mathrm{GaAs}} \simeq (\Re[\tau^{\mathrm{s}}]/\Re[\tau^{\mathrm{p}}])A$. From the value of the ellipticity A, the degree of circular polarization P_{circ}, the difference in the numbers between RCP and LCP photons, can be written as,

$$P_{\mathrm{circ}} \equiv \frac{I^{+} - I^{-}}{I^{+} + I^{-}} = \frac{2A}{1 + A^{2}}, \tag{13}$$

where I^{+} and I^{-} are the intensities of the RCP and LCP light, respectively. The degree of circular polarization $P_{\mathrm{circ}}^{\mathrm{GaAs}}$ of the light injected into the GaAs layer is shown in Fig. 6(d), which is obtained from the ellipticity shown in Fig. 6(b) using Eq. (13). Here, notable is that the degree of circular polarization $P_{\mathrm{circ}}^{\mathrm{GaAs}}$ of the light injected into the GaAs layer is proportional to the electron spin polarization generated by the circularly polarized light. The propagation of the circularly polarized light also changes the intensity of the light as $I_{\mathrm{t}}^{\mathrm{GaAs}} = T^{\mathrm{s}} I_{\mathrm{i}}^{\mathrm{s}} + T^{\mathrm{p}} I_{\mathrm{i}}^{\mathrm{p}}$. Figure 6(c) shows the light ellipticity A dependence of the intensity I_{t}^{GaAs} of the light injected into the GaAs layer obtained from

$$I_{\mathrm{t}}^{\mathrm{GaAs}} = \left(T^{\mathrm{s}} \frac{A^{2}}{1 + A^{2}} + T^{\mathrm{p}} \frac{1}{1 + A^{2}} \right) I_{\mathrm{i}}. \tag{14}$$

Here, $I_{\mathrm{i}} = I_{\mathrm{i}}^{\mathrm{s}} + I_{\mathrm{i}}^{\mathrm{p}}$ is the illuminated light intensity. Since the electric voltage due to the photoinduced ISHE is expected to be proportional to the intensity of the absorbed light, or the number of spin-polarized carriers generated by the circularly polarized light, one should calculate $(V^{\mathrm{R}} - V^{\mathrm{L}})/I_{\mathrm{t}}^{\mathrm{GaAs}}$ to compare the electric voltage induced by the circularly polarized light for different A. The $P_{\mathrm{circ}}^{\mathrm{GaAs}}$ dependence of $(V^{\mathrm{R}} - V^{\mathrm{L}})/I_{\mathrm{t}}^{\mathrm{GaAs}}$ is shown in Fig. 6(e). As shown in Fig. 6(e), $(V^{\mathrm{R}} - V^{\mathrm{L}})/I_{\mathrm{t}}^{\mathrm{GaAs}}$ is proportional to $P_{\mathrm{circ}}^{\mathrm{GaAs}}$, or the electron spin polarization. This is consistent with the prediction of the photoinduced ISHE. Thus both the light illumination angle and light ellipticity dependence of the electric voltage support that the electric voltage is induced by the ISHE driven by photoinduced spin-polarized carriers.

n_0	n_1	n_2	θ_0 (deg)	d_1 (nm)	λ (nm)
1.00	$2.12 - 4.00i$	$3.79 - 0.157i$	65	5	670

Table 2. The parameters used in the calculation. n_0, n_1, and n_2 are the complex refractive indices for air, Pt, and GaAs, respectively (Adachi, 1993; Ordal, 1983). θ_0 is the incident angle of the illumination to the normal axis of the film plane. d_1 is the thickness of the Pt layer and λ is the wavelength of the light.

T^{s}	τ^{s}	T^{p}	τ^{p}
0.249	$0.168 + 0.0200i$	0.715	$0.287 + 0.00589i$

Table 3. The transmittance $T^{\mathrm{s(p)}}$ and the transmission coefficient $\tau^{\mathrm{s(p)}}$ for the Pt/GaAs hybrid structure.

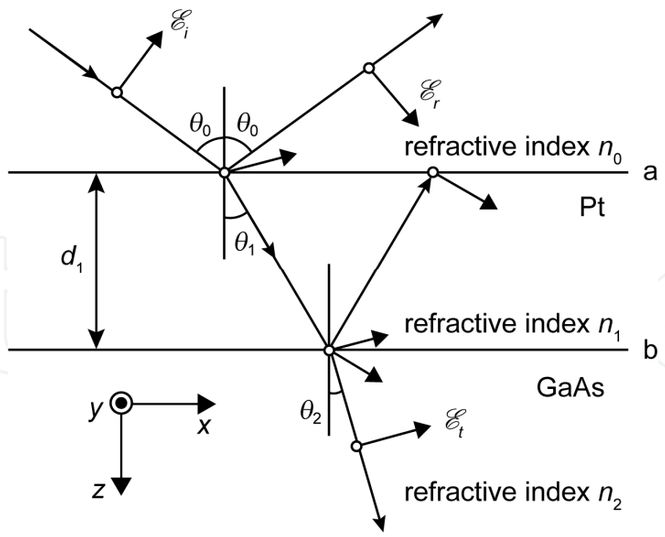

Fig. 7. The definition of θ_0, θ_1, and θ_2.

The photoinduced ISHE allows direct conversion of the circular-polarization information P_{circ} of the illuminated light into an electric voltage. The relation between $V^{\text{R}} - V^{\text{L}}$ and the circular-polarization information P_{circ} of the illuminated light can be argued from the linear dependence of $(V^{\text{R}} - V^{\text{L}}) / I_{\text{t}}^{\text{GaAs}}$ on $P_{\text{circ}}^{\text{GaAs}}$ shown in Fig. 6(e). For simplicity, we assume that the imaginary parts of n_2 and $\tau^{\text{s(p)}}$ are negligibly small: $n_2 \equiv \Re[n_2]$ and $\tau^{\text{s(p)}} \equiv \Re[\tau^{\text{s(p)}}]$ [see Tables 2 and 3]. From Eqs. (11), (12), (13), and (14), one obtains

$$I_{\text{t}}^{\text{GaAs}} = \left((\tau^{\text{s}})^2 \frac{A^2}{1+A^2} + (\tau^{\text{p}})^2 \frac{1}{1+A^2} \right) \frac{n_2 \cos\theta_2}{n_0 \cos\theta_0} I_{\text{i}}, \tag{15}$$

$$P_{\text{circ}}^{\text{GaAs}} = \frac{2\tau^{\text{s}}\tau^{\text{p}} A}{(\tau^{\text{p}})^2 + (\tau^{\text{s}})^2 A^2}, \tag{16}$$

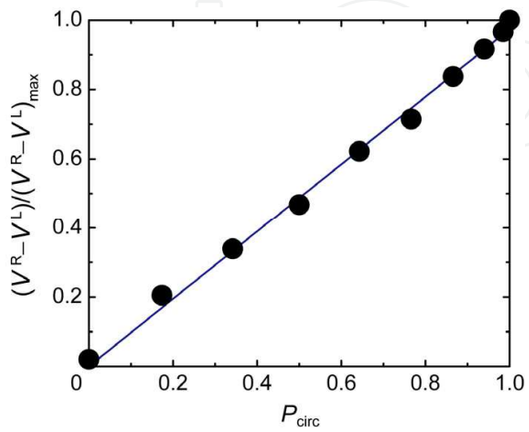

Fig. 8. The degree of circular polarization of the illuminated light ellipticity A of the illuminated light P_{circ} dependence of $V_{\text{R}} - V_{\text{L}}$.

and thus

$$V^{\mathrm{R}} - V^{\mathrm{L}} = \left(Q \frac{\tau^{\mathrm{s}} \tau^{p} n_2 \cos\theta_2}{n_0 \cos\theta_0} I_{\mathrm{i}} \right) P_{\mathrm{circ}}. \tag{17}$$

Here, $Q \equiv (V^{\mathrm{R}} - V^{\mathrm{L}}) / (I_{\mathrm{t}}^{\mathrm{GaAs}} P_{\mathrm{circ}}^{\mathrm{GaAs}})$ is the proportionality constant as seen from Fig. 6(e) and we used $A^{\mathrm{GaAs}} \simeq (\tau^{\mathrm{s}} / \tau^{\mathrm{p}}) A$. Since the proportionality constant Q is proportional to $\sin\theta_2$ because of Eq. (9), we obtain

$$V^{\mathrm{R}} - V^{\mathrm{L}} = (Q' \tau^{\mathrm{s}} \tau^{\mathrm{p}} \cos\theta_2 \tan\theta_0 I_{\mathrm{i}}) P_{\mathrm{circ}}, \tag{18}$$

where $Q \equiv Q' \sin\theta_2 = Q'(n_0 / n_2) \sin\theta_0$. Equation (18) shows that, in spite of the inequalities of $I_{\mathrm{t}}^{\mathrm{GaAs}} \neq I_{\mathrm{i}}$ and $P_{\mathrm{circ}}^{\mathrm{GaAs}} \neq P_{\mathrm{circ}}$ due to the presence of the top Pt layer and oblique illumination, the output signal $V^{\mathrm{R}} - V^{\mathrm{L}}$ is proportional to the degree of circular polarization P_{circ} of the illuminated light outside the sample. This indicates that the photoinduced ISHE can be used as a spin photodetector: the direct conversion of circular polarization information into electric voltage. This function is demonstrated experimentally in Fig. 8, in which $V^{\mathrm{R}} - V^{\mathrm{L}}$ is proportional to the degree of circular polarization of the illuminated light outside the sample.

6. Conclusion

The photoinduced inverse spin Hall effect provides a simple way for detecting light circular polarization through a spin current. This phenomenon enables the direct conversion of light-polarization information into electric voltage in a Pt/GaAs junction. This technique will be useful both in spintronics and photonics, promising significant advances in optical technology.

7. Acknowledgment

The authors thank to M. Morikawa, T. Trypiniotis, Y. Fujikawa, C. H. W. Barnes, and H. Kurebayashi for valuable discussions.

8. References

Adachi, S. (1993). *Properties of Aluminium Gallium Arsenide*, Inspec.

Ando, K., Takahashi, S., Harii, K., Sasage, K., Ieda, J., Maekawa, S. & Saitoh, E. (2008). Electric manipulation of spin relaxation using the spin Hall effect, *Physical Review Letters* Vol. 101: 036601.

Ando, K., Morikawa, M., Trypiniotis, T., Fujikawa, Y., Barnes, C. H. W. & Saitoh, E. (2010). Photoinduced inverse spin Hall effect Conversion of light-polarization information into electric voltage, *Applied Physics Letters* Vol. 96: 082502.

Hilton, D. J. & Tang, C. L. (2002). Optical orientation and femtosecond relaxation of spin-polarized holes in GaAs, *Physical Review Letters* Vol. 89: 146601.

Kimel, A. V., Bentivegna, F., Gridnev, V. N., Pavlov, V. V., Pisarev, R. V. & Rasing, T. (2001). Room-temperature ultrafast carrier and spin dynamics in GaAs probed by the photoinduced magneto-optical Kerr effect, *Physical Review* B Vol. 63:235201.

Kimura, T., Otani, Y., Sato, T., Takahashi, S. & Maekawa, S. (2007). Room-temperature reversible spin Hall effect, *Physical Review Letters* Vol. 98: 156601.

Meier F. & Zakharchenya, B. P. (1984). *Optical orientation*, North-Holland.

Ordal, M. A., Long, L. L., Bell, R. J., Bell, S. E., Bell, R. R., Alexander, J. R. W. & Ward, C. A. (1983). Optical properties of the metals Al, Co, Cu, Au, Fe, Pb, Ni, Pd, Pt, Ag, Ti, and W in the infrared and far infrared, *Applied Optics* Vol. 22: 1099.

Saitoh, E., Ueda, M., Miyajima, H. & Tatara, G. (2006). Conversion of spin current into charge current at room temperature: Inverse spin Hall effect, *Applied Physics Letters* Vol. 88: 182509.

Valenzuela, S. O. & Tinkham, M. (2006). Direct electronic measurement of the spin Hall effect, *Nature* Vol. 442: 176.

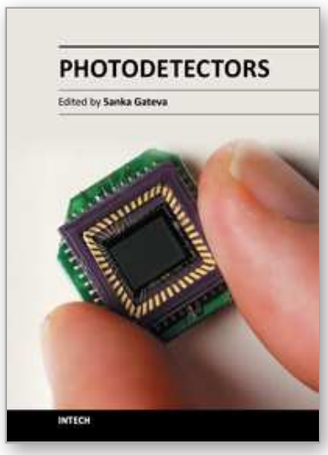

Photodetectors

Edited by Dr. Sanka Gateva

ISBN 978-953-51-0358-5
Hard cover, 460 pages
Publisher InTech
Published online 23, March, 2012
Published in print edition March, 2012

In this book some recent advances in development of photodetectors and photodetection systems for specific applications are included. In the first section of the book nine different types of photodetectors and their characteristics are presented. Next, some theoretical aspects and simulations are discussed. The last eight chapters are devoted to the development of photodetection systems for imaging, particle size analysis, transfers of time, measurement of vibrations, magnetic field, polarization of light, and particle energy. The book is addressed to students, engineers, and researchers working in the field of photonics and advanced technologies.

How to reference

In order to correctly reference this scholarly work, feel free to copy and paste the following:

Kazuya Ando and Eiji Saitoh (2012). Spin Photodetector: Conversion of Light Polarization Information into Electric Voltage Using Inverse Spin Hall Effect, Photodetectors, Dr. Sanka Gateva (Ed.), ISBN: 978-953-51-0358-5, InTech, Available from: http://www.intechopen.com/books/photodetectors/spin-photodetector-conversion-of-light-polarization-information-into-electric-voltage-using-inverse-

INTECH
open science | open minds

InTech Europe
University Campus STeP Ri
Slavka Krautzeka 83/A
51000 Rijeka, Croatia
Phone: +385 (51) 770 447
Fax: +385 (51) 686 166
www.intechopen.com

InTech China
Unit 405, Office Block, Hotel Equatorial Shanghai
No.65, Yan An Road (West), Shanghai, 200040, China
中国上海市延安西路65号上海国际贵都大饭店办公楼405单元
Phone: +86-21-62489820
Fax: +86-21-62489821

IntechOpen